JOURNAL OF CATALYSIS 109, 329–346 (1988)

A Mechanism for Sodium Oxide Catalyzed CO_2 Gasification of Carbon

JOHN M. SABER,* KEITH B. KESTER,[1,*] JOHN L. FALCONER,[2,*] AND LEE F. BROWN†

*Department of Chemical Engineering, University of Colorado, Boulder, Colorado 80309-0424, and †Isotope and Nuclear Chemistry Division, Los Alamos National Laboratory, Los Alamos, New Mexico 87545

Received June 8, 1987; revised September 1, 1987

Temperature-programmed reaction was used to study sodium oxide catalyzed CO_2 gasification of ^{13}C. The stoichiometry of the reaction is

$$CO_2 + a^{13}C \leftrightarrow CO + (1 - a)^{13}CO_2 + (2a - 1)^{13}CO,$$

where the factor a is dependent on CO_2 conversion. This stoichiometry is consistent with a mechanism composed of a reversible catalyst oxidation step and an irreversible catalyst reduction step. On the surface the catalytic surface species is oxidized by CO_2 and forms CO; during the reduction reaction the oxidized species decomposes. The reversible oxidation step, which incorporates substrate carbon into gas-phase carbon dioxide, is at equilibrium. Carbon monoxide, via the reverse of the oxidation reaction, inhibits gasification of the substrate by decreasing the number of oxidized catalytic sites on the surface. The catalyst appears both to increase the amount of oxygen on the surface and to decrease the activation energy of the reduction reaction. Similar mechanisms describe potassium- and calcium-catalyzed gasification, but Na_2CO_3 does not interact with the carbon surface as readily as K_2CO_3 does. A similar mechanism is also consistent with steam gasification results reported by others and shows that a separate water-gas shift reaction is not required for CO_2 production.

INTRODUCTION

This paper presents a mechanism (reaction steps, catalyst stoichiometries) for the sodium oxide catalyzed CO_2 gasification of carbon. Although the group IA carbonates and other oxygen-bearing salts catalyze carbon gasification reactions (*1–3*), the mechanisms of these reactions have yet to be understood completely. Recent investigations (*4–10*) suggest that alkali metal oxides catalyze carbon gasification via an oxygen transfer or oxidation–reduction mechanism. Though it appears that the process involves a cyclic oxidation and reduction of the catalytic species, many fundamental questions about the process are unanswered.

Langmuir (*11*) first proposed an oxygen-transfer mechanism for the uncatalyzed carbon–carbon dioxide reaction in 1915, and it has gained general acceptance (*12*) in one form or another. Langmuir proposed the following:

$$CO_2 + C \rightarrow (CO)_{ads} + CO \quad (1)$$

$$(C)_{ads} \rightarrow CO \quad (2)$$

with reaction (2) as the rate-limiting step. This mechanism implies that the CO molecule produced in reaction (1) contains the carbon atom from the CO_2 molecule. Bonner and Turkevich (*13*) showed this to be the case by reacting $^{14}CO_2$ with ^{12}C at temperatures below those required for reaction (2). On freezing out the reacted $^{14}CO_2$, they observed that the specific radioactivity (emissions per unit volume) of the remaining gas was the same as that of the original carbon dioxide. Thus, during uncatalyzed gasification, all the ^{14}C that reacted produced a gas-phase product containing ^{14}C.

[1] On leave from Department of Chemistry, Colorado College, Colorado Springs, CO.

[2] To whom correspondence should be addressed.

0021-9517/88 $3.00

This work was later supported by Orning and Sterling (*14*), who showed that at temperatures below those required for gasification, insignificant amounts of carbon exchanged between either $^{14}CO_2$ or ^{14}CO and a carbon surface. Reif (*12*) also showed that carbon monoxide formed immediately on CO_2 chemisorption.

Carbon monoxide inhibition of the uncatalyzed reaction has been studied extensively. Gadsby *et al.* (*15*) proposed that CO inhibits the reaction by adsorbing on the carbon,

$$CO \leftrightarrow (CO)_{ads}, \qquad (3)$$

and thus blocking adsorption of CO_2. Reif (*12*) reinterpreted Gadsby *et al.*'s data and concluded that CO inhibited gasification via the reverse of reaction (1). Reif (*12*), in his own experiments, showed that CO adsorption on the carbon was much slower than the rate of the reverse of reaction (1). Finally, Ergun (*16*) showed that the equilibrium constant of reaction (1) increased rapidly with increasing temperature. This caused the concentration of oxidized sites to increase rapidly with temperature. Since the gasification rate is proportional to the number of occupied sites, the equilibrium of reaction (1) has a pronounced effect on the rate of gasification.

To determine if a similar oxygen-transfer mechanism describes alkali metal oxide catalyzed CO_2 gasification of carbon, we used temperature-programmed desorption and reaction (TPD and TPR (*17*)), mass-spectrometric detection of products, and ^{13}C-labeling of the reactants. Temperature programming separates reaction steps in time (and temperature), and isotopic labeling allows the reaction pathways of carbon from different sources (carbonate, CO_2, CO, or carbon substrate) to be followed.

Based on these experiments, a reaction mechanism is proposed that explains many of the fundamental chemical processes of the catalyzed gasification process. The catalyst is shown to exist in two oxidation states. Both CO inhibition of the reaction and the production of carbon dioxide containing substrate carbon are shown to be the result of reversible oxidation of the catalyst. This reversible step is shown to be at equilibrium, and the catalyst reduction step (decomposition of the catalytic intermediate to form carbon monoxide) is thus rate limiting. The mechanism accurately predicts the CO_2 conversion at which formation of carbon dioxide from the substrate reaches a maximum, and it predicts the magnitude of that maximum. The results presented here have implications in the interpretation of mechanistic studies of the steam gasification of carbon.

EXPERIMENTAL METHODS

Several reaction systems were studied, but the setup and technique were similar for all (*4, 5*). In most runs, mixtures of carbon and sodium carbonate (typically 100 mg carbon and 10 mg carbonate mixed dry) were heated at a rate of 1 K/s from 300 K to 1350 K in a quartz downflow reactor in flowing He (TPD) or 10% CO_2/He (TPR). Some of these mixtures, after being heated in He or CO_2, were subsequently heated in 10% CO_2/He. Because of the experimental arrangement (*17*), the amplitudes of the product signals are proportional to the rates of reaction, and the areas under the curves are proportional to the amounts of products formed.

Gaseous products were continuously analyzed immediately downstream of the reactor with a computer-aided mass spectrometer. This arrangement allowed the time, the temperature of the carbon–catalyst mixture, and signals for labeled and unlabeled carbon monoxide and carbon dioxide to be recorded concurrently. For simplicity, ^{12}C and ^{16}O will be designated in most cases without superscripts. Concentrations of chemical species will be designated with brackets.

The mass spectrometer was calibrated daily by injection of known amounts of CO and CO_2 into the gas stream. The CO_2 and $^{13}CO_2$ cracking fractions at masses 28 and

29 and the concentrations of naturally occurring isotopes were subtracted from the appropriate signals.

Devitrification (crystallization) of the quartz, which occurs during volatilization of elemental alkali metals (*18*), was observed in most runs. As a result, the reactor walls became brittle, and a new reactor was used for each experiment.

Materials

Sterling RX-76 carbon black (Cabot Corporation), a thermally formed, oil-based black, was used for experiments requiring unlabeled carbon. According to Cabot, this carbon contained 0.5% ash, 1.5% sulfur, 0.5–1.0% oxygen, and a few ppm of heavy metals (*19*). We measured an oxygen content of approximately 200 μmol O/g C or 0.64 wt%, as described earlier (*4*).

Research-grade, isotopically labeled ^{13}C (Isotec Corporation) was specified as 99 atom% ^{13}C with Fe, 0.4 atom% (1.8 wt%), as the major contaminant. Separate experiments on this ^{13}C showed that this iron was not catalyzing gasification; the ^{13}C exhibited the same gasification activity as carbon with no iron. Other contaminants were Ca (<0.01 wt%), Na (<0.01 wt%), and K (<0.01 wt%). Isotopically labeled $Na_2^{13}CO_3$ (Prochem Corporation) was specified as 90 atom% ^{13}C. Unlabeled sodium carbonate was research grade (Baker).

The helium was UHP grade (99.999%) from Scientific Gas Products (SGP). The gas mixtures, 10% CO_2/He, 3% CO_2/He, and 10% CO/He were made from UHP gases (SGP), and their compositions were verified. The carbon dioxide calibration gas was UHP grade (99.995%), and the carbon monoxide calibration gas was CP grade (99.5%).

Experimental Procedures

Temperature-programmed desorption. To determine if the sodium catalyst cycled between oxidized and reduced forms, as proposed for oxygen transfer mechanisms (*5–10*), $Na_2^{13}CO_3$–^{12}C mixtures were heated in He (100 cm^3/min). The oxygen that was emitted on heating appeared as carbon monoxide and carbon dioxide and these were measured. The sample was then cooled to 800 K and oxidized by exposure to CO_2 at this temperature. Oxygen uptake was determined by reheating the mixture to 1350 K in He and measuring how much additional oxygen desorbed. Subsequently, the solid mixtures were analyzed with atomic absorption to determine their sodium content, because some metal was lost during the heating and cooling cycles.

Temperature-programmed reaction in CO_2. A mixture of $Na_2^{12}CO_3$ and $Na_2^{13}CO_3$ was heated in a CO_2 flow (100 cm^3/min) to study both the exchange of isotopes between the carbonate and CO_2 in the absence of carbon and the reaction of molten carbonate with the quartz reactor. The unlabeled carbonate in the mixture was used to increase the bed depth to cover the tip of the thermocouple.

In other experiments, mixtures of ^{13}C-labeled sodium carbonate and Sterling carbon black were heated in CO_2 to determine the Na : O ratio after carbonate decomposition in CO_2 flow. To isolate and distinguish steps in the gasification mechanism, mixtures of carbonate and ^{13}C were heated in CO_2. To avoid contributions to the TPR spectra from carbonate decomposition, the mixtures were first heated in CO_2 flow to 1350 K and then cooled to 300 K. Data were obtained during subsequent heating in CO_2 to 1350 K.

Pulse experiments. In an attempt to explain the source of $^{13}CO_2$ produced during CO_2 gasification of ^{13}C, ^{13}CO was pulsed into CO_2 that was flowing over a mixture of ^{12}C and sodium catalyst. The sodium catalyst was formed by heating a mixture of carbon and sodium carbonate to 1350 K in He and then exposing it to CO_2. The experiment was done at several temperatures from 295 to 1223 K.

Temperature-programmed reaction in CO. To elucidate how carbon monoxide inhibits catalyzed carbon dioxide gasification

of carbon, flowing 10% CO/He was reacted with both reduced and oxidized forms of the catalyst on ^{13}C substrates. The reduced form of the catalyst was made by heating a mixture of carbonate and ^{13}C to 1350 K and then cooling it to 300 K, all in flowing He. The oxidized form of the catalyst was prepared by cooling the mixture from 1350 to 800 K in He, then cooling the mixture in CO_2 from 800 K to room temperature.

RESULTS

Sodium Carbonate in CO_2 Flow

During heating of a mixture of 28 mg $Na_2^{13}CO_3$ and 102 mg $Na_2^{12}CO_3$ in a CO_2 flow, ^{13}C from the carbonate appeared in the gas phase as $^{13}CO_2$, starting at 650 K (Fig. 1). Below 1100 K the $^{13}CO_2$ signal was accompanied by a decrease, rather than an increase, in the $^{12}CO_2$ signal. Apparently $^{12}CO_2$ exchanged with the carbon and oxygen in the carbonate. Between 650 K and

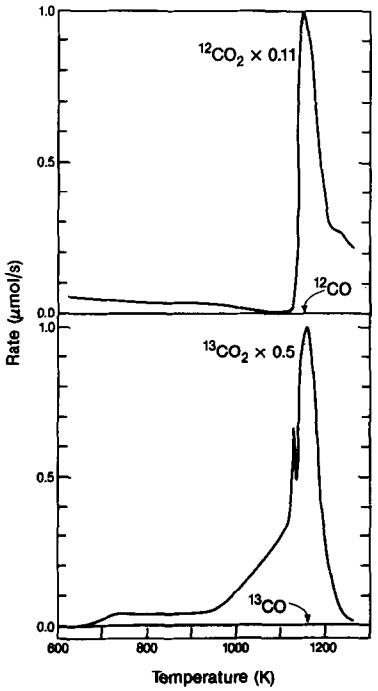

FIG. 1. Temperature-programmed desorption spectra for a mixture of 102 mg $Na_2^{12}CO_3$ and 28 mg $Na_2^{13}CO_3$ in 10% CO_2/He flow. The zero on the rate scale for the $^{12}CO_2$ signal corresponds to 10 μmol/s.

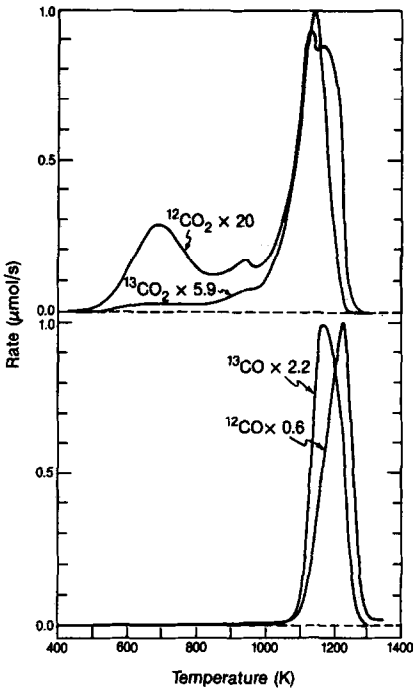

FIG. 2. Temperature-programmed desorption spectra for a mixture of 10 mg $Na_2^{13}CO_3$ and 100 mg Sterling carbon black in He flow.

1124 K (Na_2CO_3 melting point), 30% of the ^{13}C from the carbonate exchanged.

As the carbonate melted, both the $^{12}CO_2$ and $^{13}CO_2$ signals increased sharply (Fig. 1); no carbon monoxide was produced. The $^{13}CO_2$ and $^{12}CO_2$ products were produced in the proportion in which the carbon isotopes were initially mixed. Since sodium carbonate does not decompose when it melts (*20*), carbon dioxide production may have been due to reaction of the liquid carbonate with the quartz reactor. The quartz devitrified more severely in this experiment than in any other.

$Na_2^{13}CO_3$ and Carbon in He Flow

When a mixture of $Na_2^{13}CO_3$ and ^{12}C was heated in a He flow (TPD), $^{12}CO_2$ and $^{13}CO_2$ formed, starting at 500 K. Most of the carbon dioxide formed above 1000 K, and above 1100 K much larger amounts of ^{12}CO and ^{13}CO were observed (Fig. 2).

The same CO_2 peak at 690 K seen in Fig. 2 was also observed during TPD of unla-

beled carbon black with no catalyst present. Since the peak shape and temperature were unaffected by sodium carbonate, the carbonate apparently does not interact significantly with the carbon surface oxides at these temperatures. This is in contrast to potassium carbonate, which modifies both the shape and temperature of the peak (*5*).

Small amounts of $^{13}CO_2$ formed under 1000 K. Above this temperature, the rate of $^{13}CO_2$ formation increased rapidly. As the $^{13}CO_2$ signal increased, ^{13}CO and ^{12}CO formed; apparently some of the $^{13}CO_2$ gasified the substrate to produce ^{13}CO and ^{12}CO.

During heating, all the oxygen reacted to produce carbon monoxide and carbon dioxide (Table 1). The oxygen that reacted included both the oxygen in the carbonate and that originally present on the carbon. The oxygen content of the carbon was determined by measuring the amounts of CO and CO_2 produced during TPD of carbon in He to 1350 K. Thus, the sodium complex that remained on the carbon in He flow apparently contained no oxygen. Since more ^{12}CO than ^{13}CO formed (Table 1), the carbonate apparently decomposed to give the elemental metal by reaction with the carbon substrate.

This complex, when cooled from 800 to 300 K in a CO_2 flow, took up one oxygen atom for each sodium atom that remained after heating to 1350 K. The oxygen uptake was determined by measuring the amount of oxygen that desorbed, as CO_2 and CO, during reheating in helium to 1350 K. The sodium content after heating was determined by atomic absorption analysis of the resulting mixture. Since the carbon alone did not take up significant amounts of oxygen (*4*), we assume that the oxygen taken up by the mixture was associated with the sodium–carbon complex. A metal : oxygen ratio of 1 was also measured for an oxidized potassium catalyst (*4*, *7*).

TABLE 1

Product Distribution during TPD of $Na_2^{13}CO_3$–^{12}C Mixtures

Product	Amount (μmol)
^{12}CO	168
$^{12}CO_2$	12
^{13}CO	55
$^{13}CO_2$	27
Total ^{13}C	82
Total O	300

Note. The original mixture contained 94 μmol $Na_2^{13}CO_3$ (85 μmol ^{13}C in carbonate due to isotope purity), 20 μmol O in Sterling carbon black, and 302 μmol atomic O total.

$Na_2^{13}CO_3$ and Carbon in $^{12}CO_2$ Flow

During TPR of $Na_2^{13}CO_3$/C in 10% CO_2/He, all of the ^{13}C in the carbonate was observed as $^{13}CO_2$; no ^{13}CO formed. The equal but opposite changes in the CO_2 and $^{13}CO_2$ signals (Fig. 3) show that the $^{13}CO_2$ formation was due to isotope exchange between gas-phase carbon dioxide and sodium carbonate rather than to decomposition of the carbonate. Note that the rate of exchange increased rapidly as the temperature approached the melting point of the carbonate.

Near 1200 K, the carbon monoxide signal was significantly larger than that expected from complete conversion of the CO_2 flow (Fig. 3). The CO overproduction was ascribed to carbonate decomposition. The carbon monoxide was unlabeled because all the original ^{13}C in the carbonate had exchanged prior to carbonate decomposition. To determine the amount of carbon monoxide that formed by carbonate decomposition and subsequent reaction of the liberated carbon dioxide with the carbon substrate, the amount of CO expected from gasification by the inlet CO_2 was subtracted from the observed ^{12}CO curve in Fig. 3. The difference between the inlet CO_2 signal and the total CO_2 signal leaving the reactor ($^{12}CO_2$ + $^{13}CO_2$), when multiplied by the reaction stoichiometry of two, corresponds to the CO signal expected due to gasification

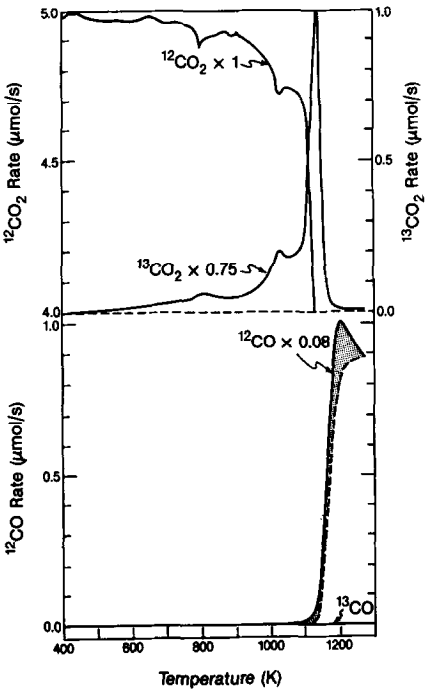

FIG. 3. Temperature-programmed desorption spectra for a mixture of 11 mg $Na_2^{13}CO_3$ and 100 mg Sterling carbon black in 10% CO_2/He flow. The dashed line is the CO signal expected from gasification, as measured from the decrease in total carbon dioxide signal. The cross-hatched area is the CO formed by carbonate decomposition.

(dashed line in Fig. 3). The cross-hatched area in Fig. 3, the difference between the observed CO signal and that expected due to gasification, is the CO formed by carbonate decomposition and reaction (248 μmol of CO). Since 124 μmol of carbonate (372 μmol O) was originally mixed with the carbon, 124 μmol of oxygen remained on the surface. Since only small amounts of CO desorbed from the carbon alone (*4*), the final Na : O ratio was 2 if no sodium vaporized during these initial stages of decomposition. The K : O ratio was also 2 after potassium carbonate decomposition on carbon in either a 10% CO_2/He or He flow (*4*).

Sodium Catalyst and ^{13}C in CO_2 Flow

By heating ^{13}C in $^{12}CO_2$ in the presence of a sodium catalyst, the separate reaction pathways of the gas-phase and substrate carbon can be followed during catalyzed gasification. Several aspects of the resulting spectra (Fig. 4) are of interest for understanding the gasification mechanism:

- $^{13}CO_2$ formed in significant quantities in a broad peak between 900 and 1200 K, and the rate of $^{13}CO_2$ production was initially greater than the rate of ^{13}CO production.
- The production rates of CO and ^{13}CO *were not the same* except at complete conversion of CO_2; between 850 and 1075 K, CO formed at a much faster rate than did ^{13}CO.
- The area between the CO and ^{13}CO curves equaled twice the area under the $^{13}CO_2$ curve.
- At all temperatures, consumption of 1 mol of $^{12}CO_2$ produced 1 mol of ^{12}CO.
- At all temperatures, the amount of oxygen flowing into the reactor as CO_2 equaled the amount of oxygen leaving the reactor as products or unreacted CO_2.
- The $[^{12}CO]/[^{12}CO_2]$ ratio equaled the $[^{13}CO]/[^{13}CO_2]$ ratio at all conversions of CO_2 (Table 2).

The same observations, where applicable, were made for repeated heating and cooling cycles and for constant temperature gasification. For instance, $^{13}CO_2$ was pro-

TABLE 2

Carbon Monoxide: Carbon Dioxide Ratios for Catalyzed Temperature-Programmed Reaction of CO_2 with ^{13}C[a]

% $^{12}CO_2$ conversion	$^{12}CO/^{12}CO_2$	$^{13}CO/^{13}CO_2$
13	0.15	0.19
17	0.21	0.23
20	0.25	0.27
30	0.43	0.45
40	0.67	0.67
50	0.99	0.99
60	1.49	1.49
70	2.27	2.29
80	3.93	4.06
90	8.90	9.25
96	22.8	23.9

[a] 10 mg Na_2CO_3 and 100 mg ^{13}C.

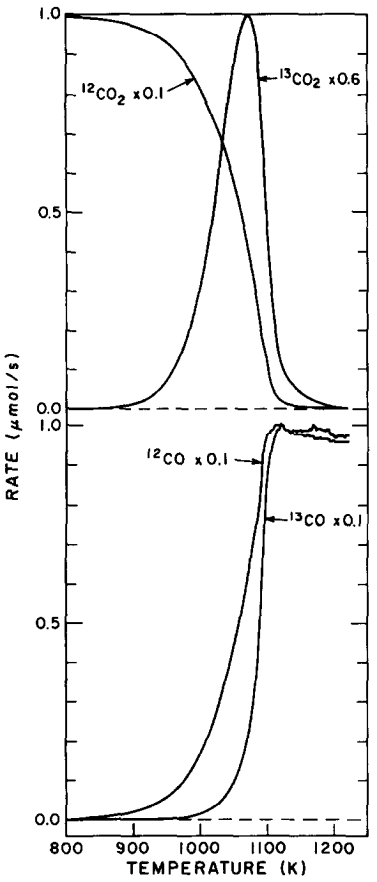

FIG. 4. Temperature-programmed reaction spectra for Na-catalyzed CO_2 gasification of ^{13}C (10 mg Na_2CO_3 and 100 mg ^{13}C) in 10% CO_2/He flow. The carbon dioxide curves are offset vertically for clarity.

duced at a constant rate at a given temperature as long as ^{13}C substrate was available for reaction. Thus, the $^{13}CO_2$ observed during TPR is due to a continuous production of $^{13}CO_2$ and not to desorption of a fixed amount of $^{13}CO_2$ from the surface.

Reactions with Carbon Monoxide

Flowing CO_2 (10 μmol/s) was passed over an isothermal mixture of unlabeled catalyst and unlabeled carbon. At several temperatures, ^{13}CO (33 μmol over a 10-s period) was injected into the CO_2 stream. As temperatures approached those required for substrate gasification, $^{13}CO_2$ formed (Table 3). Since the ^{13}CO was the only source of ^{13}C, the $^{13}CO_2$ production was a result of ^{13}CO consumption. Above 1100 K, the $[CO]/[CO_2]$ ratio approximately equaled the $[^{13}CO]/[^{13}CO_2]$ ratio.

The reaction (TPR) of flowing ^{12}CO with the oxidized catalyst on ^{13}C (prepared by decomposing carbonate on ^{13}C in He and then reoxidizing it in $^{12}CO_2$) produced 27 μmol $^{12}CO_2$ between 600 and 1200 K but no detectable amounts of $^{13}CO_2$ (Fig. 5). Because of the relatively high concentration of ^{12}CO, small changes in the ^{12}CO signal were not detected. Above 900 K, ^{12}CO reacted with the ^{13}C to produce ^{13}CO.

Reaction of flowing CO with the reduced catalyst on ^{13}C (prepared by heating the carbonate–carbon mixture in a He flow) produced neither CO_2 nor $^{13}CO_2$ above the background level at any temperature. Above 1000 K, however, ^{13}CO was produced. At 1100 K, the reaction rate to form ^{13}CO was only 0.2% of the gasification rate of ^{13}C by CO_2.

DISCUSSION

Isotope Exchange and Carbon/Carbonate Interactions

Isotope exchange reactions with carbon dioxide are common on many metal oxides (*21*, *22*) and are thought to proceed through the formation of surface carbonate ions

TABLE 3

Carbon Monoxide: Carbon Dioxide Ratios When ^{13}CO Was Pulsed into CO_2 That Was Flowing over ^{12}C[a]

T (K)	$^{12}CO/^{12}CO_2$	$^{13}CO/^{13}CO_2$	% ^{13}CO consumed
295	0.03	>400	0
573	0.04	>400	0
638	0.04	>400	0
726	0.07	384	<1
834	0.09	14	7
952	0.10	5.2	10
1066	0.43	1.3	42
1121	1.2	1.4	41
1163	1.7	1.7	37
1223	3.9	3.9	20

[a] Sterling carbon black (100 mg) and sodium catalyst (10 mg carbonate).

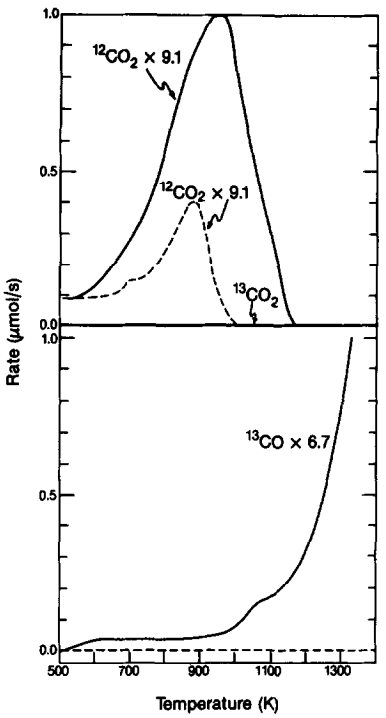

FIG. 5. Temperature-programmed reaction of an oxidized Na/^{13}C mixture in 10% CO/He flow. The dashed line is $^{12}CO_2$ formed when the mixture was heated in He flow.

(*21*). Carbon and oxygen isotopes are also known to exchange between gas-phase CO_2 and $K_2^{13}CO_3$ on carbon (*5*). The exchange with sodium carbonate, however, is significantly slower than with potassium carbonate. Over 90% of the exchange with potassium occurs below 1000 K, but less than 10% does for sodium. The $^{12}CO_2$ peak near 650 K in Fig. 2 is the same as that obtained from Sterling carbon black alone. Though sodium carbonate does not modify this peak, potassium carbonate completely changes it. Apparently at low temperatures potassium carbonate interacts with carbon surface oxides (*4*) but sodium carbonate does not.

The rapid increase in the rate of exchange between CO_2 and sodium carbonate on carbon occurs near the melting point of the carbonate. This isotope exchange is slower (and not complete) in the absence of carbon. As evidenced by severe devitrification of the quartz, the molten carbonate probably reacts with the quartz reactor.

Catalyst Stoichiometry

For oxygen-transfer mechanisms, the catalyst complex is thought to cycle between two oxidation states. We determined that sodium carbonate on carbon decomposed in CO_2 flow to form a species with the stoichiometry of Na_2O. When sodium carbonate on carbon was decomposed in He and then reoxidized by CO_2, the final Na:O ratio was 1. These two oxidation states of the catalyst complex, both observed in the presence of CO_2, are used in the mechanism. The same stoichiometries were obtained for potassium under similar conditions (*4*). Thus, the carbonate is not the active form of the catalyst for these alkali metals (*4, 23–25*).

Although the stoichiometries of the catalytic species are those of sodium oxide (Na_2O) and sodium peroxide (Na_2O_2), the structures of the catalytic complexes with carbon surfaces are not known. Metal oxides are known to promote both homomolecular and heteromolecular isotope exchange reactions (*21, 22*) such as the ones we observed. Thus, Na_2O could exist as a separate entity on the carbon surface. We observed, however, that granular Na_2O_2, when mixed with carbon powder, decomposed to produce carbon monoxide near 1000 K; in contrast, bulk Na_2O_2 decomposed at 733 K. This suggests that carbon and admixed Na_2O_2 form a complex below 733 K.

Reaction Mechanism

We have suggested (*26*) reactions (4)–(6) as a possible mechanism for $^{12}CO_2$ gasification of ^{13}C. This mechanism will be shown to be consistent with the extensive experimental results presented here. The first step is oxidation of the catalytic site by CO_2; the second step is reduction of the catalytic site by the ^{13}C substrate. The third step is the

reverse of the first step, but written for $^{13}CO_2$.

catalyst oxidation: (1) $[Na_2O{-}^{13}C + CO_2(g) \leftrightarrow (NaO)_2{-}^{13}C + CO(g)]$ (4)

catalyst reduction: (*a*) $[(NaO)_2{-}^{13}C + {}^{13}C \rightarrow Na_2O{-}^{13}C + {}^{13}CO(g)]$ (5)

catalyst reduction: $(1 - a)[(NaO)_2{-}^{13}C + {}^{13}CO(g) \leftrightarrow Na_2O{-}^{13}C + {}^{13}CO_2(g)]$ (6)

The overall reaction is the sum of these steps:

$$CO_2(g) + a^{13}C \leftrightarrow CO(g) + (1 - a)^{13}CO_2(g) + (2a - 1)^{13}CO(g) \quad (7)$$

The factors (1, a, $1 - a$) that multiply the reaction steps indicate the numbers of times that the steps must occur to yield the overall reaction, Eq. (7). If a is the fraction of the net amount of $(NaO)_2{-}^{13}C$ formed in reaction (4) that reacts to form gaseous carbon monoxide in reaction (5), then in order to maintain a constant concentration of $(NaO)_2{-}^{13}C$, the rest $(1 - a)$ must be reduced by carbon monoxide in reaction (6). The cumulative factor a at the reactor exit (a_f) is a function of CO_2 conversion, X_f, as shown in Appendix A [$a_f = 1/(2 - X_f)$]. The same reaction sequence is observed for K, Ba (*27*), and Ca (*28*) catalysts.

This mechanism is both a refinement and an extension of oxidation–reduction mechanisms previously proposed for uncatalyzed and catalyzed gasification. For the uncatalyzed reaction, Gadsby *et al.* (*15*) suggested the following mechanism:

$$CO_2(g) + C \rightarrow CO(a) + CO(g) \quad (8)$$

$$CO(a) \leftrightarrow CO(g) \quad (9)$$

Many other researchers (*11–14, 16, 29*) proposed a similar mechanism, but with reaction (8) being reversible.

Kapteijn and Moulijn (*23*) proposed a two-step oxidation–reduction mechanism for the alkali metal-catalyzed reaction

$$(M_xO_y){-}C + CO_2(g) \leftrightarrow (M_xO_{y+1}){-}C + CO(g) \quad (10)$$

$$(M_xO_{y+1}){-}C + C \leftrightarrow (M_xO_y){-}C + CO(g), \quad (11)$$

where M is an alkali metal. The mechanism we propose is similar to that of Kapteijn and Moulijn, but we have identified the catalyst stoichiometries, introduced a step to explain $^{13}CO_2$ formation, and shown that the first step in the sequence is reversible and at equilibrium.

The oxidized and reduced forms of the catalyst in Kapteijn and Moulijn's mechanism may be different for different alkali metals (*6, 23*), although our work suggests that Na and K catalysts have the same two M : O ratios for the oxidized and reduced forms of the catalyst. An explanation of the reaction mechanism and how our data are consistent with it is presented below.

Catalyst Oxidation

The catalyst oxidation step [Eq. (4)] forms one mole of ^{12}CO for each mole of $^{12}CO_2$ that reacts, as observed experimentally. Additionally, when $Na{-}^{13}C$ (formed during heating in He) was oxidized by CO_2 at 800 K to form $(NaO)_2{-}^{13}C$, the only gas-phase reaction product was ^{12}CO; no ^{13}CO formed. Thus, oxidation is a separate step from reduction [Eq. (5)]. Oxidation proceeds at 800 K, but reduction only has a significant rate at higher temperatures. This is similar to uncatalyzed gasification, where the oxygen exchange step [Eq. (8)] has been shown to occur at temperatures significantly lower than the onset of the desorption step [Eq. (9)] (*13*).

The oxidation step is reversible. During TPR experiments with flowing CO (Fig. 5), the oxidized catalyst was reduced by CO by the reverse of reaction (4),

$$(NaO)_2{-}^{13}C + CO \leftrightarrow Na_2O{-}^{13}C + CO_2 \quad (12)$$

The maximum rate of this reaction was lower in 10% CO/He (0.11 μmol CO_2 produced/s) than in 10% CO_2/He (1.6 μmol $^{13}CO_2$ produced/s). This is consistent with the proposed mechanism, which predicts

that the concentration of $(NaO)_2$–^{13}C species will decrease with time in the CO atmosphere, but $(NaO)_2$–^{13}C will be continually regenerated in CO_2. The production of CO_2 during TPR in flowing CO was not the result of CO disproportionation,

$$2\ CO \rightarrow CO_2 + C, \qquad (13)$$

because CO_2 production slowed as the oxidized catalyst was consumed.

These experiments show directly that a reversible oxidation step occurs, as proposed by Kapteijn and Moulijn (*23*) and Koenig *et al.* (*8*). The results are also consistent with the work of Yokoyama *et al.* (*24*) and Koenig *et al.* (*8*), who showed that carbon monoxide reacts with oxidized alkali metal catalysts on carbon surfaces to produce CO_2. They did not report, however, whether the carbon substrate or the gas-phase CO was the source of the carbon ultimately found in the CO_2. The oxidation reaction is considered reversible in uncatalyzed gasification also (*12–14, 16*).

Catalyst Reduction

The reduction step, reaction (5), appears to be rate-limiting since it occurs only at temperatures well above those required for oxidation of the reduced form of the catalyst. Additionally, the onset of gasification in CO_2 occurs at 850 ± 10 K. This is the same temperature that we observed for the onset of $(NaO)_2$–^{13}C decomposition in He. Moreover, as shown below, the oxidation step is in equilibrium at gasification temperatures.

A rate-limiting reduction step has been proposed by others (*1, 3, 8, 23–25*). Kapteijn and Moulijn (*23*), for instance, observed an overproduction of CO when the atmosphere above the reduced form of a potassium catalyst, at reaction temperature, was changed from He to CO_2. They proposed that the overproduction was due to an initial, rapid oxidation of the catalyst and that the decrease to a lower steady-state rate occurred because the rate was limited by the reduction step.

The reduction step appears to be essentially irreversible since we were unable to oxidize the reduced form of the catalyst with CO. When the oxidized catalyst was exposed to CO, production of CO_2 decreased to zero as the oxidized catalyst was reduced. If the reduction step [Eq. (5)] were reversible, CO disproportionation [Eq. (13)] would occur in a two-step process as CO oxidized Na_2O–^{13}C,

$$Na_2O\text{–}^{13}C + CO \rightarrow (NaO)_2\text{–}^{13}C + C, \qquad (14)$$

and the oxidized species then formed CO_2 via reaction (12). The disproportionation reaction does not proceed over the reduced catalyst, however, since no carbon dioxide formed in this experiment. Consumption of ^{12}CO in this manner is also in consistent with the production of one ^{12}CO molecule for each $^{12}CO_2$ molecule consumed during gasification.

Production of $^{13}CO_2$

Carbon dioxide gasification of ^{13}C produced $^{13}CO_2$ (Fig. 4) by reaction (6), which is the reverse of reaction (4) but written for ^{13}C-labeled gas-phase reactants. The reasons for this conclusion follow.

When ^{13}CO was pulsed into $^{12}CO_2$ that was flowing over ^{12}C, $^{13}CO_2$ was produced. This came from reaction (6). At high CO_2 conversions, moreover, the $[^{13}CO]/[^{13}CO_2]$ ratio equaled the $[^{12}CO]/[^{12}CO_2]$ ratio, as observed during CO_2 gasification of ^{13}C. The most plausible explanation for this is that reaction (6) is in equilibrium and is the principal device for producing $^{13}CO_2$. Because the catalyst oxidation step [reaction (4)] is reversible, at least some $^{13}CO_2$ would be expected when reaction (6) consumes ^{13}CO that is produced by reaction (5). The equilibrium of reaction (6) shows that this is the principal factor in the production of $^{13}CO_2$. Therefore, additional reaction steps, such as isotope exchange of carbon dioxide,

$$CO_2 + (NaO)_2\text{–}^{13}C \leftrightarrow {}^{13}CO_2 + (NaO)_2\text{–}C, \qquad (15)$$

are not required to account for $^{13}CO_2$ production.

The sum of reactions (4) and (6) yields the oxygen-transfer reaction,

$$CO_2 + {}^{13}CO \leftrightarrow {}^{13}CO_2 + CO \quad (16)$$

This reaction has been described (*30–32*) by two-step mechanisms such as

$$CO_2 + (*) \leftrightarrow CO + (O)_{ads} \quad (17)$$

$$^{13}CO + (O)_{ads} \leftrightarrow {}^{13}CO_2 + (*) \quad (18)$$

where * is an active oxygen-transfer site. Because the oxidation step is reversible, the oxygen-transfer reaction is an inherent part of the gasification mechanism. Oxygen transfer between CO and H_2O (water-gas shift reaction) and between deuterated water and hydrogen molecules are described by similar mechanisms (*33*).

Reaction Equilibrium

If the oxidation step is in equilibrium, as expected when the reduction step is rate determining, then the following are true for reactions (4) and (6):

$$k_1[Na_2O{-}{}^{13}C][{}^{12}CO_2] \approx k_{-1}[(NaO)_2{-}{}^{13}C][{}^{12}CO] \quad (19)$$

$$k_1[Na_2O{-}{}^{13}C][{}^{13}CO_2] \approx k_{-1}[(NaO)_2{-}{}^{13}C][{}^{13}CO], \quad (20)$$

where the same set of rate constants is used for both reactions. Chemical exchange ^{12}C–^{13}C separation factors (*34*) and ratios of rate constants for reactions using ^{12}C and ^{13}C (*35*) indicate that both equilibrium and kinetic isotope effects were less than the experimental variation in our work. Dividing Eq. (19) by Eq. (20), then canceling and rearranging, yields

$$[{}^{12}CO]/[{}^{12}CO_2] \approx [{}^{13}CO]/[{}^{13}CO_2], \quad (21)$$

where the bracketed values are the effluent concentrations. During reaction of CO_2 with ^{13}C, the $[CO]/[CO_2]$ ratio approximately equaled the $[^{13}CO]/[^{13}CO_2]$ ratio at all CO_2 conversions (Table 2). This equality is a direct consequence of the equilibrium of reactions (4) and (6). Because of errors due to mass spectrometer sensitivity and resolution and because of corrections for cracking fractions and isotopic purities, the smallest signals have the largest percentage errors. Thus, the largest percentage deviations from Eq. (21) would be expected at the highest and lowest conversions of CO_2. Since the largest deviations are observed at the extreme conversions of CO_2 (Table 2), the approximate equality of the ratios may indeed be closer than those reported.

The maximum rate of $^{13}CO_2$ production was approximately 17% of the CO_2 flow rate into the reactor and occurred at 58 or 59% conversion of the inlet CO_2. These values were the same for the three CO_2 flow rates used (3, 5, and 10 μmol/s), for two CO_2 concentrations (3 and 10% CO_2/He), and for Na-, K-, and Ca-catalyzed reactions (Table 4). As shown in Appendix A, these are the expected values if reactions (4) and (6) are in equilibrium. The maximum flow rate of $^{13}CO_2$ is calculated to occur at a CO_2 conversion of 58.6%, and the maximum flow rate of $^{13}CO_2$ is calculated to be 17.2% of the inlet CO_2 flow rate. The values are independent of inlet flow rate or concentration, as observed. These values are also independent of catalyst or catalyst loading if the oxidation step is at equilibrium. Since the same percentages were measured for Na, K, and Ca catalysts (Table 4), the oxidation reaction is at equilibrium for all three catalysts. Thus the experimentally observed maximum $^{13}CO_2$ production rate and

TABLE 4

Maximum $^{13}CO_2$ Production Rate and Fractional $^{12}CO_2$ Conversion at This Maximum Rate

Catalyst[a]	Inlet gas composition	$^{12}CO_2$ conversion (%)	$R_{max}(^{13}CO_2)/F_i$[b]
Na	3% CO_2/He	58	0.17
Na	10% CO_2/He	59	0.16
K	10% CO_2/He	58	0.16
Ca	10% CO_2/He	58	0.16

[a] 10 mg carbonate and 100 mg ^{13}C.

[b] $R_{max}(^{13}CO_2)$ is the maximum rate of $^{13}CO_2$ formation and F_i is flow rate of CO_2 into reactor.

the $^{12}CO_2$ conversion where this occurred agree exactly with theoretical predictions. The predictions were based on the reaction sequence presented in Eqs. (4)–(6). This agreement between the theoretical predictions and experimental observations is regarded as extremely strong support for the proposed mechanism.

That these values are not experimental artifacts is shown by the reaction of CO_2 with HCl-washed ^{13}C (*36*). Although the overall reaction has the same stoichiometry as the alkali metal-catalyzed reaction, the $[^{12}CO]/[^{12}CO_2]$ ratio *did not equal* the $[^{13}CO]/[^{13}CO_2]$ ratio. Additionally, the maximum flow rate of $^{13}CO_2$ was only 2% of the inlet flow rate of CO_2 and occurred at 85% conversion of CO_2.

Delay in ^{13}CO Production

The delay in net production of ^{13}CO relative to ^{12}CO (Fig. 4) is a direct result of consumption of ^{13}CO to produce $^{13}CO_2$. At the lower temperatures and lower $^{12}CO_2$ conversions, the equilibrium of reaction (6) favors $^{13}CO_2$ formation (Table 2). Thus, some of the ^{13}CO produced by decomposition of $(NaO)_2$–^{13}C reacts by reaction (6) to produce $^{13}CO_2$; this decreases the yield of ^{13}CO. The difference between the CO and ^{13}CO signals is equal to twice the $^{13}CO_2$ signal. The factor of 2 is caused by the two oxygen atoms necessary to make one $^{13}CO_2$ molecule, compared with the one necessary to make a ^{13}CO molecule. Thus, as expected from our mechanism, the difference between the ^{12}CO and ^{13}CO signals should equal twice the $^{13}CO_2$ signal, as observed. The delay was also observed for K and Ca catalysts, since these reactions also have the oxidation step at equilibrium.

Carbon Monoxide Inhibition

Inhibition of the gasification reaction by CO occurs because the reverse of the oxidation reaction consumes the oxidized catalytic species. Since gasification is limited by decomposition of $(NaO)_2$–^{13}C, a decrease in its concentration results in a lower gasification rate.

In contrast, the reverse of reaction (5) appears to be slow and not responsible for CO inhibition. During TPR (CO flow) of a mixture of ^{13}CO and the oxidized catalyst, only the reverse of oxidation [reaction (4)] was observed. That is, CO_2 was formed, and that reaction ceased once the catalyst was reduced. At higher temperatures, ^{12}CO reacted to form ^{13}CO (Fig. 5),

$$^{12}CO + {}^{13}C \leftrightarrow {}^{13}CO + {}^{12}C. \quad (22)$$

This reaction can proceed by the reverse of reaction (5),

$$^{12}CO + Na_2O\text{–}{}^{13}C \rightarrow (NaO)_2\text{–}{}^{13}C + {}^{12}C. \quad (5a)$$

Then, the forward reaction forms ^{13}CO as $(NaO)_2$–^{13}C reacts with ^{13}C via reaction (5),

$$(NaO)_2\text{–}{}^{13}C + {}^{13}C \rightarrow Na_2O\text{–}{}^{13}C + {}^{13}CO. \quad (5)$$

At 1100 K, the rate of reaction (22), and thus of (5a), was 0.02 μmol/s, and the rate of reduction reaction (5) was 10 μmol/s. As a result, the exchange of carbon between gaseous CO and the substrate carbon is kinetically insignificant during CO_2 gasification of carbon.

Catalytic Activity

A recent study by Freund (*37*) indicated that the catalyst serves only to increase the number of active sites. In contrast, a study by Koenig *et al.* (*8*) showed that not only does the catalyst increase the number of active sites, it also lowers the activation energy. Kapteijn *et al.* (*6*) reinterpreted Freund's data and concluded that alkali metal catalysts serve both to increase the active site density and to lower the activation energy for desorption of CO.

For both potassium (*4, 7*) and sodium catalysts, one oxygen atom is present for each metal atom on the surface when the catalyst has been exposed to carbon diox-

ide, but carbon alone takes up insignificant amounts of oxygen under the same conditions (*4*). The rate of substrate gasification is enhanced by the increased concentration of reactive-oxygen sites on the surface.

Koenig *et al.* (*8*) and Yokoyama *et al.* (*24*) showed that the catalyst increases the amount of surface oxygen by increasing the rate of CO_2 absorption. The rate constant for CO_2 dissociation, however, remains the same. The large increase in surface oxygen is thought to weaken carbon–carbon bonds by withdrawing electrons from the carbon matrix (*8, 24*). Therefore, the activation energy for desorption of carbon monoxide that contains substrate carbon decreases. Several studies (*38–40*) reported that the activation energy for gasification decreased with increasing catalyst weight loading.

In our study, the activation energy of the rate-limiting step was obtained from the change in the concentrations of ^{13}CO and $^{13}CO_2$ with temperature. As shown in Appendix B, the sum of these two concentrations is proportional to the rate that ^{13}C is gasified. An Arrhenius plot for the rate of reaction (5) yielded an activation energy of 180 kJ/mol (Table 5). The activation energies of the K- and Ca-catalyzed reactions are similar, and all are less than the activation energy of the uncatalyzed reaction (*36*).

TABLE 5

Activation Energies for ^{13}C Gasification

Catalyst[a]	Activation energy of reaction (5) (kJ/mol)
$CaCO_3$	210
Na_2CO_3	180
K_2CO_3	170
Uncatalyzed (Ref. (*36*))	270

[a] 100 mg ^{13}C and 10 mg carbonate.

Steam Gasification of Carbon

Taylor and Neville (*41*) proposed a mechanism for steam gasification in which CO and H_2 formed in the first step,

$$C + H_2O \leftrightarrow CO + H_2 \qquad (23)$$

With excess steam, the water-gas shift reaction occurred,

$$CO + H_2O \leftrightarrow CO_2 + H_2 \qquad (24)$$

and carbon dioxide then reacted with the carbon to produce carbon monoxide,

$$C + CO_2 \leftrightarrow 2\ CO \qquad (25)$$

The resulting CO could react with the excess steam to yield additional carbon dioxide and hydrogen.

Taylor and Neville (*41*) concluded that CO_2 gasification [reaction (25)] was the rate-limiting step because the same materials catalyzed both steam and CO_2 gasification. This was mechanistically reasonable because increasing the rate that CO_2 reacts with carbon decreases the concentration of CO_2 and increases the concentration of CO. Both these changes shift reaction (24) toward production of more hydrogen and more consumption of H_2O.

Others (*12, 40, 42*) have suggested that H_2O and CO_2 gasification proceed by similar oxygen-transfer reactions. Our work supports such a mechanism for steam gasification:

$$(1)\quad [H_2O + Na_2O\text{–}C \leftrightarrow H_2 + (NaO)_2\text{–}C] \qquad (26)$$

$$(a)\quad [(NaO)_2\text{–}C + C \rightarrow Na_2O\text{–}C + CO] \qquad (27)$$

$$(1-a)\quad [CO + (NaO)_2\text{–}C \leftrightarrow CO_2 + Na_2O\text{–}C] \qquad (28)$$

$$H_2O + aC \leftrightarrow H_2 + (1-a)\ CO_2 + (2a-1)\ CO \qquad (29)$$

This stoichiometry (Eq. 29) was observed by Wigmans *et al.* (*40*) for steam gasification and is similar to what we observed for CO_2 gasification. Mims and Pabst (*42*) suggested that reduction step (27) is rate limiting for potassium-catalyzed steam gasification. This is rate limiting for CO_2 gasification also. Thus, the same materials should be effective catalysts for both reactions, as observed (*1*).

Reaction (28) is in equilibrium for CO_2 gasification of carbon and thus may be in equilibrium during steam gasification also. Therefore, contrary to what is generally assumed (*43, 44*), a separate water-gas shift reaction is not needed to form CO_2. Indeed, Wigmans *et al.* (*40*) showed unequivocally, by different experimental approaches, that the water-gas shift reaction was not in equilibrium during potassium-catalyzed steam gasification of their carbon. If the reduction step [reaction (27)] is the rate-limiting step, and the water-gas shift reaction was the source of the observed product CO_2, then it would be expected that the shift would be in equilibrium. The fact that it was not in equilibrium for these investigators' experiments indicates that the water-gas shift was not responsible for CO_2 production in their experiments.

In contrast to the results of Wigmans *et al.* (*40*), Mims and Pabst (*42*) reported that reaction (26) is at equilibrium. They flowed D_2 and H_2O over a catalyst/carbon mixture, froze the water products out of the effluent stream, and analyzed the remaining gas with a mass spectrometer. They concluded that reaction (26) was at equilibrium since D_2, HD, and H_2 were statistically scrambled. The rate of the exchange was zero order in H_2O, however, rather than first order as predicted by their model. They may have measured the rate of H_2–D_2 exchange rather than the rate of equation (26); they did not determine the isotopic distribution in the water products.

While Wigmans *et al.* (*40*) showed that the water-gas shift reaction was not the source of product CO_2, they did not suggest that the CO_2 came from a reaction of gas-phase CO with the catalyst; rather, they suggested that an adsorbed oxide species reacted with the oxidized catalyst to form gaseous CO_2 and the reduced catalyst. Our work, on the other hand, suggests that the reaction of gas-phase CO with the oxidized catalyst to form the reduced catalyst and gas-phase CO is the true source of CO_2 produced in the steam gasification of carbon.

Reactions (26)–(29) also explain why an increase in CO partial pressure in the inlet gas increases the rate of H_2O consumption in steam gasification but decreases the rate of CO_2 consumption in CO_2 gasification. The ratio of reduced sites to oxidized sites is dependent on the $[CO]/[CO_2]$ ratio. An increase in CO partial pressure increases the number of reduced catalytic sites available for reaction with CO_2 or H_2O. For CO_2 gasification, the CO_2 concentration increases with an increase in CO concentration because of the equilibrium of reaction (4). During steam gasification, however, an increase in the number of reduced catalytic sites with which the water can react increases the rate of H_2O consumption. According to Eqs. (26)–(28), however, the rate of *carbon* consumption will decrease because CO decreases the number of oxidized catalytic sites, the decomposition of which gasifies the carbon.

CONCLUSIONS

A mechanism that involves catalyst oxidation and reduction accurately describes CO_2 gasification of carbon for sodium, potassium, and calcium catalysts. The oxidation step is reversible and at equilibrium, and thus incorporates substrate carbon into gas-phase carbon dioxide. Carbon monoxide, via the reversible oxidation reaction, inhibits gasification of the substrate by decreasing the number of oxidized catalytic sites on the carbon surface. The reduction step is essentially irreversible and thus rate-determining. The catalyst increases the amount of oxygen on the surface and decreases the activation energy for desorption

of carbon monoxide that contains substrate carbon. A similar oxygen-transfer mechanism adequately describes catalyzed steam gasification and shows that the water-gas shift reaction is not required for CO_2 production.

APPENDIX A: SIGNIFICANCE OF PARAMETER a IN ANALYSIS OF CATALYZED CARBON OXIDATION

The significance of the parameter a and its relationship to conversion is developed for the plug-flow reactor used in this study. The rates r of the three reaction steps [Eqs. (4)–(6)] are defined in terms of substances that occur only in the particular reaction: i.e., the rate of the catalyst oxidation step [Eq. (4)] is defined in terms of $r_{^{12}CO_2}$, because $^{12}CO_2$ appears only in the catalyst oxidation step. Similarly, the rate of the first catalyst reduction step [Eq. (5)] is defined in terms of $r_{^{13}C}$, and the rate of the second catalyst reduction step [Eq. (6)] in terms of $r_{^{13}CO_2}$.

The parameter a is defined as the fraction of times the first reduction step occurs for every time the oxidation step occurs. For the plug flow reactor the *measured* a is an integrated value, and is designated as a_f.

$$a_f = \frac{\int_0^{V_r} (r_{^{13}C})dV}{\int_0^{V_r} (r_{^{12}CO_2})dV} \tag{A1}$$

The rates $r_{^{13}C}$, and $r_{^{12}CO_2}$ are negative, since both reactants are consumed.

At steady state for the three reaction steps, a carbon-12 balance yields

$$-r_{^{12}CO_2} = r_{^{12}CO}, \tag{A2}$$

an oxygen balance yields

$$-r_{^{12}CO_2} = \tfrac{1}{2}r_{^{12}CO} + \tfrac{1}{2}r_{^{13}CO} + r_{^{13}CO_2}, \tag{A3}$$

and a carbon-13 balance yields

$$-r_{^{13}C} = r_{^{13}CO} + r_{^{13}CO_2}. \tag{A4}$$

Substituting Eq. (A2) into (A3) and simplifying yields

$$-r_{^{12}CO_2} = r_{^{13}CO} + 2r_{^{13}CO_2}. \tag{A5}$$

Eliminating $r_{^{13}CO}$ from Eqs. (A4) and (A5) yields

$$r_{^{13}CO_2} = -r_{^{12}CO_2} + r_{^{13}C}. \tag{A6}$$

Integrating Eq. (A6) over the reactor volume V_r gives

$$\int_0^{V_r} (r_{^{13}CO_2})dV = \int_0^{V_r} (-r_{^{12}CO_2})dV + \int_0^{V_r} (r_{^{13}C})dV. \tag{A7}$$

Dividing both sides of Eq. (A7) by $\int_0^{V_r} (-r_{^{12}CO_2})dV$ yields

$$\frac{\int_0^{V_r} (r_{^{13}CO_2})dV}{\int_0^{V_r} (-r_{^{12}CO_2})dV} = 1 - \frac{\int_0^{V_r} (r_{^{13}C})dV}{\int_0^{V_r} (r_{^{12}CO_2})dV} = 1 - a_f. \tag{A8}$$

Eq. (A8) shows that the fraction of times the second catalyst reduction step [Eq. (6)] occurs for every time the catalyst oxidation step occurs is $(1 - a_f)$.

As shown in Eq. (21),

$$\frac{[^{12}CO]}{[^{12}CO_2]} \approx \frac{[^{13}CO]}{[^{13}CO_2]}. \tag{A9}$$

The concentrations of ^{12}CO and $^{12}CO_2$ can be expressed in terms of fractional conversion X, inlet flow rate of $^{12}CO_2$ (F_0), and the volumetric flow rate q:

$$q[^{12}CO_2] = F_0(1 - X), \tag{A10}$$

and from Eq. (A2),

$$q[^{12}CO] = F_0(X), \tag{A11}$$

Dividing Eq. (A11) by (A10) yields

$$\frac{[^{12}CO]}{[^{12}CO_2]} = \frac{X}{1 - X}. \tag{A12}$$

At the reactor exit, where measurements are made, the ratio $[^{13}CO]/[^{13}CO_2]$ can be expressed in terms of a_f. Integration of Eq. (A4) gives

$$\int_0^{V_r} (-r_{^{13}C})dV = \int_0^{V_r} (r_{^{13}CO})dV + \int_0^{V_r} (r_{^{13}CO_2})dV. \quad \text{(A13)}$$

Dividing this through by $\int_0^{V_r} (r_{^{12}CO_2})dV$ gives

$$\frac{\int_0^{V_r} (-r_{^{13}C})dV}{\int_0^{V_r} (r_{^{12}CO_2})dV} = \frac{\int_0^{V_r} (r_{^{13}CO})dV}{\int_0^{V_r} (r_{^{12}CO_2})dV} + \frac{\int_0^{V_r} (r_{^{13}CO_2})dV}{\int_0^{V_r} (r_{^{12}CO_2})dV}. \quad \text{(A14)}$$

Substituting equivalences from Eqs. (A1) and (A8) into Eq. (A14) and rearranging yields

$$\frac{\int_0^{V_r} (r_{^{13}CO})dV}{\int_0^{V_r} (-r_{^{12}CO_2})dV} = 2a_f - 1. \quad \text{(A15)}$$

Since $q_f[^{13}CO]_f = \int_0^{V_r} (r_{^{13}CO})dV$

and $q_f[^{13}CO_2]_f = \int_0^{V_r} (r_{^{13}CO_2})dV$, (A16)

then from Eqs. (A8) and (A15),

$$\frac{[^{13}CO]_f}{[^{13}CO_2]_f} = \frac{\int_0^{V_r} (r_{^{13}CO})dV}{\int_0^{V_r} (r_{^{13}CO_2})dV} = \frac{2a_f - 1}{1 - a_f}. \quad \text{(A17)}$$

Equations (A9) (using an exact equality for the approximate equality), (A12), and (A17) can now be combined to give

$$X_f = (2a_f - 1)/a_f \quad \text{and} \quad a_f = 1/(2 - X_f). \quad \text{(A18)}$$

The molar flow rate of $^{13}CO_2$ leaving the reactor is equal to $q_f[^{13}CO_2]_f$. If q_f is regarded as a very weak function of temperature, then the maximum production rate of $^{13}CO_2$ is reached at the temperature where $[^{13}CO_2]_f$ is a maximum. A value of the conversion X_f where the production rate of $^{13}CO_2$ is a maximum can be derived as follows.

From Eq. (A8), the production rate of $^{13}CO_2$ can be set equal to $(1 - a_f)$ times the amount of $^{12}CO_2$ converted:

$$\int_0^{V_r} (r_{^{13}CO_2})dV = (1 - a_f) \int_0^{V_r} (-r_{^{12}CO_2})dV \quad \text{(A19)}$$

or

$$q_f[^{13}CO_2]_f = (1 - a_f)(F_0)(X_f). \quad \text{(A20)}$$

Substituting the expression for X_f from Eq. (A18) and dividing through by q_f gives

$$[^{13}CO_2]_f = \left[\frac{F_0}{q_f}\right]\left[\frac{(1 - a_f)(2a_f - 1)}{a_f}\right]. \quad \text{(A21)}$$

To locate the temperature at which the maximum exit concentration of $^{13}CO_2$ occurs, the derivative of Eq. (A21) is taken with respect to temperature and set equal to zero:

$$\frac{d[^{13}CO_2]_f}{dT} = \left[\frac{F_{^{12}CO_2}}{q_f}\right]\left[\frac{-2a_f^2 + 1}{a_f^2}\right]\left[\frac{da_f}{dT}\right] = 0. \quad \text{(A22)}$$

Thus, since the other terms on the right side cannot be zero,

$$-2a_f^2 + 1 = 0, \quad \text{and} \quad a_f = 1/\sqrt{2} \quad \text{(A23)}$$

at the point where the exiting concentration of $^{13}CO_2$ reaches a maximum. Substituting this value into Eq. (A18) yields

$$X_f = 1 - \sqrt{2} = 0.586 \quad \text{(A24)}$$

at the temperature where the exiting concentration of $^{13}CO_2$ reaches a maximum. The maximum flow rate of $^{13}CO_2$ is obtained from Eq. (A21) for $a_f = 1/\sqrt{2}$:

$$q_f[^{13}CO_2]_f = 0.172\ F_0. \quad \text{(A25)}$$

APPENDIX B: DETERMINATION OF ACTIVATION ENERGY

Values of $\int_0^{V_r} (r_{^{13}C})dV$ were obtained from measurements of $q_f[^{13}CO_2]_f$ and $q_f[^{13}CO]_f$. Since

$$q_f[^{13}CO]_f = \int_0^{V_r} (r_{^{13}CO})dV \quad \text{and}$$

$$q_f[^{13}CO_2]_f = \int_0^{V_r} (r_{^{13}CO_2})dV, \quad \text{(B1)}$$

combining these with Eq. (A13) yields

$$\int_0^{V_r} (-r_{^{13}C})dV = q_f[^{13}CO]_f + q_f[^{13}CO_2]_f. \quad \text{(B2)}$$

The activation energies E presented in the text were obtained from the slope of ln $[\int_0^{V_r} (-r_{^{13}C})dV]$ as a function of $1/T$. This was obtained by plotting the logarithm of $([^{13}CO] + [^{13}CO_2])$ versus inverse temperature.

Since

$$r_{^{13}C} = -A_2 \exp[-E_2/RT][\theta], \quad \text{(B3)}$$

where A_2 is the preexponential factor of reaction (2) and θ is the fraction of catalytic sites that are oxidized,

$$\frac{d\left[\ln \int_0^{V_r} (-r_{^{13}C})dV\right]}{d(1/T)} = \frac{d(\ln A_2)}{d(1/T)} - \frac{E}{R} + \frac{d \ln \left[\int_0^{V_r} (\theta)dV\right]}{d(1/T)} \quad \text{(B4)}$$

Equation (19), written in terms of θ, becomes

$$k_1(1 - \theta)[^{12}CO_2] = k_{-1}\theta[^{12}CO]. \quad \text{(B5)}$$

The preexponential factor is assumed to be independent of temperature, so the first term on the right side of Eq. (B4) is zero. If this is solved for θ, K_1 substituted for k_1/k_{-1}, and the expression for the ratio $[^{12}CO]/[^{12}CO_2]$ from Eq. (A12) substituted, the result is

$$\theta = \frac{K_1}{K_1 + [X/(1 - X)]}. \quad \text{(B6)}$$

When K_1 is large, or X is small, $\theta \approx 1$. If $\theta \approx 1$ throughout the experimental range, then the third term on the right side of Eq. (B5) is approximately zero, and the activation energy of reaction (5) is obtained from the indicated plot.

Below reaction temperature, the reduced catalyst, when exposed to CO_2, emits one mole of CO for each mole of sodium on the carbon surface. No further oxidation or reduction occurs until the onset of the reaction at about 850 K. This indicates that θ remains at 1 until 850 K. At higher temperatures, Eq. (B6) indicates that a point will be reached where θ becomes less than 1, either because of the change in X as conversion increases or because of a possible decrease in K_1. When this happens, the third term on the right side of Eq. (B5) becomes positive, and the plot from which the activation energy is determined curves. Experimentally, this usually occurred at about 80% conversion. The activation energies reported in the text were measured at conversions well below this value; this implies that they were obtained in the region where θ is approximately one. The reported activation energies thus represent the true activation energies of the rate-limiting steps of the catalyzed oxidations.

ACKNOWLEDGMENTS

We gratefully acknowledge the support by the Department of Energy, Pittsburgh Energy Technology Center (Grant DE-FG22-82PC50798). We thank Kevin G. Wilson for his help with the computer system, and Keith M. Bailey for writing part of the data collection routine. We are especially grateful to Willy Grothe for instrument construction, and to Norman W. Taylor for electronic construction and computer interfacing.

REFERENCES

1. Walker, P. L., Jr., Shelef, M., and Anderson, R. A., *Chem. Phys. Carbon* **4,** 287 (1968).
2. Krupp, British Patent 8426 (1892).
3. Taylor, H. S., and Neville, H. A., *J. Amer. Chem. Soc.* **43,** 2055 (1931).
4. Saber, J. M., Falconer, J. L., and Brown, L. F., *Fuel* **65,** 1356 (1986).
5. Saber, J. M., Falconer, J. L., and Brown, L. F., *J. Catal.* **90,** 65 (1984).
6. Kapteijn, F., Peer, O., and Moulijn, J. A., *Fuel* **65,** 1371 (1986).
7. Hashimoto, K., Miura, K., Xu, J.-J., Watanabe, A., and Masukami, H., *Fuel* **65,** 489 (1986).
8. Koenig, P. C., Squires, R. G., and Laurendeau, N. M., *J. Catal.* **100,** 228 (1986).

9. Ferguson, E., Schlogl, R., and Jones, W., *Fuel* **63,** 1048 (1984).
10. Dunks, G. B., Stelman, D., and Yosim, S. J., *Carbon* **18,** 365 (1980).
11. Langmuir, I., *J. Amer. Chem. Soc.* **37,** 1156 (1915).
12. Reif, A. E., *J. Phys. Chem.* **56,** 785 (1952).
13. Bonner, F., and Turkevich, J., *J. Amer. Chem. Soc.* **73,** 561 (1951).
14. Orning, A. A., and Sterling, E., *J. Phys. Chem.* **58,** 1044 (1954).
15. Gadsby, J., Long, F. J., Sleightholm, P., and Sykes, K. W., *Proc. R. Soc. London A* **193,** 357 (1948).
16. Ergun, S., *J. Phys. Chem.* **60,** 480 (1956).
17. Falconer, J. L., and Schwarz, J. A., *Catal. Rev. Sci. Eng.* **25,** 141 (1983).
18. McKee, D. W., and Chatterji, D., *Carbon* **16,** 53 (1978).
19. Cabot Corp. Tech. Rep. S-36 and private communication, Paul Baurgault, Cabot Corp. (1986).
20. "CRC Handbook of Chemistry and Physics," 67th Ed. CRC Press, Boca Raton, FL, 1986.
21. Kasatkina, L. A., and Antoshin, G. V., *Kinet. Katal.* **4,** 252 (1962).
22. Winter, E. R. S., *J. Amer. Chem. Soc.*, p. 5781 (1967).
23. Kapteijn, F., and Moulijn, J. A., *Fuel* **62,** 221 (1983).
24. Yokoyama, S., Miyahara, K., Tanaka, K., Takakuwa, I., and Tashiro, J., *Fuel* **58,** 510 (1979).
25. Moulijn, J. A., Cerfontain, M. B., and Kapteijn, F., *Fuel* **63,** 1043 (1984).
26. Saber, J. M., Falconer, J. L., and Brown, L. F., *J. Chem. Soc. Chem. Commun.*, p. 445 (1987).
27. Ersolmaz, C., and Falconer, J. L., *Fuel* **65,** 400 (1986).
28. Adcock, J. P., and Falconer, J. L., unpublished results.
29. Evropin, B. A., Kulkova, N. B., and Temkin, M. I., *Zh. Fiz. Khim.* **30,** 348 (1948).
30. Stroeva, S. S., Kul'kova, N. V., and Temkin, M. I., *Dokl. Akad. Nauk. SSSR* **124,** 628 (1959).
31. Frank-Kamenetskii, D. A., *Dokl. Akad. Nauk. SSSR* **23,** 662 (1939).
32. Semechkova, A. F., and Frank-Kamenetskii, D. A., *Zh. Fiz. Khim.* **19,** 291 (1941).
33. Temkin, M. I., Nakhmanovich, M. L., and Morozov, N. M., *Kinet. Katal.* **2,** 722 (1961).
34. Bigeleisen, J., "Isotope Effects in Chemical Processes," ACS Advances in Chemistry Series No. 89, pp. 1–24. Amer. Chem. Soc., Washington, D.C., 1969.
35. Fry, A., "Isotope Effects in Chemical Reactions," ACS Monograph No. 167, pp. 354–414. Van Nostrand–Reinhold, New York, 1970.
36. Saber, J. M., Ph.D. Thesis, University of Colorado, 1987.
37. Freund, H., *Fuel* **64,** 657 (1985).
38. Huhn, F., Klein, J., and Juentgen, H., *Fuel* **62,** 196 (1983).
39. Veraa, M. J., and Bell, A. T., *Fuel* **57,** 194 (1978).
40. Wigmans, T., Elfring, R., and Moulijn, J. A., *Carbon* **21,** 1 (1983).
41. Taylor, H. S., and Neville, H. A., *J. Amer. Chem. Soc.* **43,** 2055 (1921).
42. Mims, C., and Pabst, J. K., *Prepr. ACS Div. Fuel Chem.* **25,** 263 (1980).
43. Cabrera, A. L., Heinemann, H., and Somorjai, G. A., *Chem. Phys. Lett.* **81,** 402 (1981).
44. McKee, D. W., and Yates, J. T., Jr., *J. Catal.* **71,** 308 (1981).